Developing a Baseline Characterization of River Bathymetry and Time-Varying Height for Chindwin River in Myanmar Using SRTM and Landsat Data

Indira Bose[1]; Susantha Jayasinghe[2]; Chinaporn Meechaiya[3]; Shahryar K. Ahmad[4]; Nishan Biswas[5]; and Faisal Hossain[6]

Abstract: In this study, a method was developed for the baseline characterization of river bathymetry and time-varying heights using globally available datasets from the Shuttle Radar Topography Mission (SRTM) elevation data and Landsat visible imagery. Using independent data on river water elevations from satellite altimetry, the SRTM-Landsat approach was verified as to how well it can work for baseline characterization. The technique was demonstrated for Chindwin River locations in Myanmar that were also independently sampled by Sentinel 3A and Jason 3 altimeters. The Modified Normalized Difference Water Index (MNDWI) was used for estimating the water areas and widths using Landsat 8 from 2016 to 2019. A comparison of SRTM-Landsat with Sentinel 3A/Jason 3–based elevation changes resulted in a correlation coefficient up to 0.89 and 0.82 using area-elevation and width-elevation curves, respectively. The presence of river islands during the dry season resulted in a weaker correlation between our proposed SRTM-Landsat technique and altimeter water elevations. This case study over the Chindwin River in Myanmar demonstrated that the use of the SRTM-Landsat combined technique could yield an acceptable baseline for characterization of river bathymetry and time-varying heights at ungauged locations around the world. **DOI: 10.1061/(ASCE)HE.1943-5584.0002126.**

Author keywords: River; Water elevations; Bathymetry satellite; Altimeter; Landsat; Shuttle Radar Topography Mission (SRTM) and Chindwin River.

Introduction

Rivers are dynamic water bodies as they change their morphology with time due to diverse natural and anthropogenic factors. The variations in a river's height, width, and course have considerable influence on natural resources and human assets. Radical changes, under severe conditions, can cause serious disasters such as floods and droughts. Most importantly, the characterization of river bathymetry and river surface elevation is critical to calibration and even the validation of hydrodynamic models for predicting or forecasting inundation and understanding flood risk. Therefore, it is vital to understand the physical attributes of rivers and their dynamics over time (Kumar et al. 2015; Gao et al. 2016; Karpatne et al. 2016; Huang et al. 2017).

One essential quantity of a river's state is the elevation of the water surface above a datum. Water surface elevation can be determined either by staff gauges (manual observation) or through automated sensors, such as pressure transducers, optical sensors, radio detection, and ranging sensors (Sauer and Turnipseed 2010). However, conventional ground-based monitoring stations are very limited, and institutional barriers further limit data sharing (Jiang et al. 2020). Lack of in situ river data constrains our ability to observe and predict hydrological events like flooding or drought and sediment transport phenomena, especially in mountain areas (Jiang et al. 2020). The temporal and spatial coverage provided by remote sensing techniques makes space-borne data attractive for river applications in ungauged regions (Neal et al. 2018; Andreadis et al. 2013; Schumann et al. 2014). The increased availability of remote sensing data has now enabled the development of new approaches for characterizing a river's bathymetry and water surface elevations (Bates et al. 2013; Paiva et al. 2015).

Over the last 25 years, microwave satellite remote sensing has provided an alternative source of water surface elevation observations to monitor water level and storage variations at a regional scale (Jiang et al. 2020; Arsen et al. 2015; Boergens et al. 2017). Microwave remote sensing has the advantage of being all-weather with day and night coverage that overcomes the continuing issues of cloud cover in optical satellite images. The Shuttle Radar Topography Mission (SRTM) that flew in February 2000 used radar interferometry to provide a robust source of dry land topographic data at a global scale to estimate river bathymetry above the water level during the SRTM overpass. However, the large variation in average terrain height precision found in the SRTM literature reveals vertical precision that is dependent on location, terrain characteristics, and surface feature properties (Schumann et al. 2008; Yamazaki et al. 2017). Several radar nadir altimetry missions, such as Jason-2

[1]Dept. of Civil and Environmental Engineering, Univ. of Washington, Seattle, WA 98195.
[2]Asian Disaster Preparedness Center, Paholyothin Rd., Phayathai, Bangkok 10400, Thailand.
[3]Asian Disaster Preparedness Center, Paholyothin Rd., Phayathai, Bangkok 10400, Thailand.
[4]Dept. of Civil and Environmental Engineering, Univ. of Washington, Seattle, WA 98195.
[5]Dept. of Civil and Environmental Engineering, Univ. of Washington, Seattle, WA 98195.
[6]Dept. of Civil and Environmental Engineering, Univ. of Washington, Seattle, WA 98195 (corresponding author). ORCID: https://orcid.org/0000-0001-6192-3157. Email: fhossain@uw.edu

Note. This manuscript was submitted on March 6, 2021; approved on June 22, 2021No Epub Date. Discussion period open until 0, 0; separate discussions must be submitted for individual papers. This paper is part of the ***Journal of Hydrologic Engineering***, © ASCE, ISSN 1084-0699.

in 2008, CryoSat-2 in 2010, SARAL in 2013, Jason-3 in 2016, Sentinel-3A in 2016, and Sentinel-3B in 2018, have been launched and successfully applied for water surface elevation determination (Biancamaria et al. 2018). These radar altimeters determine the distance from the satellite to a target surface by measuring the round-trip travel time for a radar pulse from satellite to surface (Aviso 2020).

Since their launch, several studies have used microwave remote sensing missions for water surface elevation estimation. Schumann et al. (2008) compared remotely-sensed water stages derived from light detection and ranging (LiDAR), topographic contours, and SRTM (Schumann et al. 2008). Maswood and Hossain (2016) used SRTM topographic data for deriving river network and flow direction and modeled the ungauged basins using satellite remote sensing for the Ganges–Brahmaputra–Meghna basin. Moramarco et al. (2019) used the entropy theory to simulate river bathymetry from remote sensing data from radar altimeters and microwave radiometers. Legleiter and Harrison (2019) used remote sensing more directly to map river depth. They reported that bathymetric LiDAR was highly accurate and precise in shallow water. However, areas with a depth of more than 2 m resulted in large gaps in coverage of estimating river depth from remote sensing. Kasvi et al. (2019) recently compared various remote sensing techniques for estimating river bathymetry. They reported that more research was needed to develop remote sensing approaches for measuring shallow water bathymetry. Many studies used Jason-2, Envisat, Jason-3, and Sentinel 3A and 3B for hydrodynamic and hydrologic models (Biancamaria et al. 2018; Getirana and Peters-Lidard 2013; Liu et al. 2015; Kittel et al. 2018, 2021). Yan et al. (2015) summarized the integration of low-cost satellite data with flood modeling, focusing particularly on the use of freely available data sets, such as digital elevation models (DEMs), radar altimeter measurements, and synthetic aperture radar (SAR) imagery. These in-depth studies conclude that the monitoring of the water area and water surface elevation are quite consistent and reliable using remote sensing data (Schumann et al. 2012; Birkinshaw et al. 2010; Bercher and Kosuth 2012).

Despite the wider availability of altimeter data today, the SRTM product is still widely used for monitoring bathymetry and water surface elevation due to the ease of availability and global coverage (Bonnema et al. 2016; Bonnema and Hossain 2017). Radar altimeters do not provide such coverage and are limited in their sampling of the world's rivers. However, the 20-year-old SRTM data have limitations as SRTM-derived bathymetry may not be representative of recent conditions, particularly for very dynamic water bodies/rivers. More importantly, information on intra and interannual variations in the water level is needed for efficient river management, which cannot be estimated with the static topographic data from SRTM. Finally, a large portion of bathymetry under the water level that was not observed by SRTM during its overpass needs to be estimated for river hydraulic applications. To address these limitations, we propose an alternative approach to generate a baseline for river bathymetry and time-varying river elevations for potential global application by combining SRTM topographic with Landsat visible data. This case study is driven by the need to address the practical limitations faced on the ground for estimating river bathymetry and height for the calibration of hydrodynamic models at ungauged regions.

The overarching question of this study was as follows:

- What is the skill of using SRTM and visible Landsat satellite imagery for estimating river bathymetry and time-varying water surface elevations when compared with independently measured river elevation from satellite altimetry?

To answer this question, our choice for independent water elevations was Sentinel 3A and Jason 3 altimeter mission data. Our proposed technique, based on the global coverage of SRTM and Landsat missions, can be potentially used as a baseline method for most world's rivers that are missed by altimeters where there is no prior information. The proposed technique can also be vital for baseline characterizations needed in river product development for the planned Surface Water and Ocean Topography (SWOT) satellite mission. SWOT is scheduled for launch in 2022, and river elevation is going to be a key and flagship product (Biancamaria et al. 2016).

Study Area

The verification of the proposed SRTM-Landsat combined method was tested over 10 virtual stations of the Chindwin River where the Sentinel 3A and Jason 3 tracks intersected (Fig. 1). Chindwin River, which is considered a lifeline for Myanmar, is a major tributary of the Ayeyarwady River. It is one of the five major rivers in Myanmar, measuring approximately 850 km in length (Shrestha et al. 2020). Chindwin River is prone to flooding, and therefore, any technique to estimate time-varying river levels can improve the calibration and validation of hydrodynamic river models required for predicting flood risk.

Data

Four satellite remote sensing products were used with different spatial, temporal, and spectral characteristics. These include the following: (1) Landsat 8 Tier 1 Surface Reflectance with 30 m spatial resolution, (2) SRTM with 30 m spatial resolution, (3) Sentinel 3A level 2 synthetic aperture radar altimeter (SRAL) Ku-band (300 m after SAR processing) and C-band with a spatial resolution of approximately 300 m, and (4) Jason 3 (water surface elevation retrieved from the Dynamic River Width based Altimeter Height Visualizer website of the SASWE research group (University of Washington) from Biswas et al. (2019). The datum of SRTM, Sentinel 3A, and Jason 3 were converted to the Earth Gravitational Model (EGM) 2008 geoid (Pavlis et al. 2012). Sentinel 3A and Jason 3 data were retrieved for a 4-year period spanning 2016 to 2019. The JavaScript API of the Google Earth Engine (GEE) platform was used for the processing of SRTM and Landsat products, which are available in the GEE data catalog. The Sentinel 3A dataset was downloaded from the Copernicus open access hub, SciHub, and the water surface elevation values were processed as described in the methodology subsection "Water Heights Derived from Sentinel 3A and Jason 3 Altimeters."

Methodology

Our proposed method for the Chindwin River in Myanmar can be broadly described as follows. As shown in Fig. 2, first, the area-elevation and width-elevation relationships using SRTM topographic data were developed for multiple reaches of the Chindwin River. Using the best-fit regression equations and Landsat-8 derived water areas and widths, the water elevations that were not observed by SRTM were estimated for the entire bathymetry. Next, time-varying water elevations were derived from 2016 to 2019 utilizing the regression equations derived from the aforementioned area-elevation and width-elevation relationships (Fig. 2).

Our proposed methodology begins first with defining a river reach that spans 1 km upstream and 1 km downstream of each

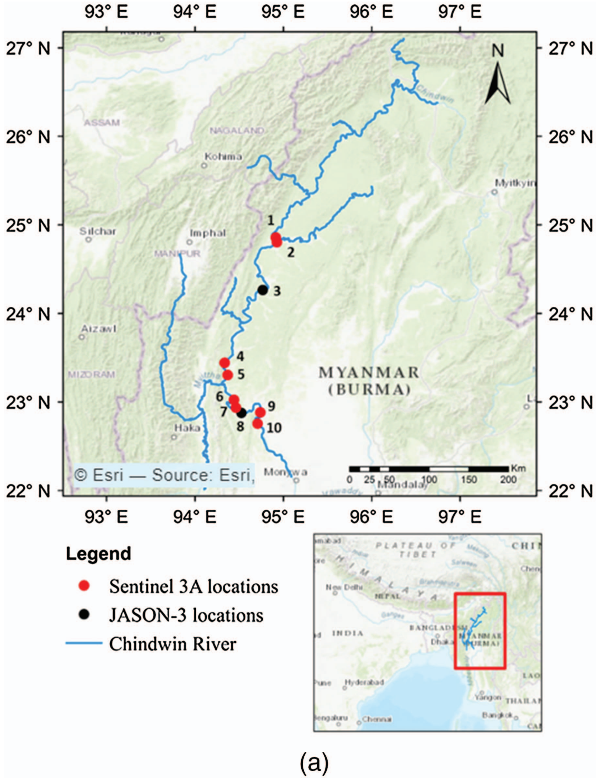

Latitude, Longitude (From upstream to downstream)
1) 24.858, 94.915 (Sentinel 3A)
2) 24.805, 94.928 (Sentinel 3A)
3) 24.266, 94.768 (JASON 3)
4) 23.443, 94.337 (Sentinel 3A)
5) 23.305, 94.371 (Sentinel 3A)
6) 23.025, 94.442 (Sentinel 3A)
7) 22.936, 94.464 (Sentinel 3A)
8) 22.888, 94.529 (JASON 3)
9) 22.882, 94.74 (Sentinel 3A)
10) 22.756, 94.709 (Sentinel 3A)

(b)

Fig. 1. (Color) Study area showing (a) Chindwin River in Myanmar and virtual stations of Sentinel 3A (red dots) and Jason 3 (black dots) tracks; and (b) latitude and longitude of each station. (Map © Esri.)

virtual station identified in Fig. 1. Next, SRTM data were processed using the GEE platform and derived area-elevation and width-elevation curves for each river reach. The relationship between each virtual station's area/width and elevation was identified using a regression model to determine the best-fit equations. Cloud-free Landsat 8 images were selected from 2016 to 2019, as well as the determined areas and widths associated with each of the 2 km river reaches, upstream and downstream, for assessing the levels throughout the year that were not captured by SRTM (Fig. 3). Using the best-fit regression equations derived from the SRTM-Landsat combined technique, water surface elevations corresponding to the concurrent Landsat areas and widths were determined. The period from 2016 to 2019 was selected because of the concurrent availability of Sentinel 3A and Jason 3 altimetric data. We extracted Sentinel 3A and Jason 3 altimeter elevations (over designated virtual stations of Fig. 1) closest to the dates of acquisition from Landsat 8 and compared the change of water surface elevations over the selected time period. The correlation coefficients between SRTM-Landsat based and Sentinel 3A/Jason 3-based water elevation changes were evaluated to verify the accuracy of our proposed technique.

SRTM-Based Area-Elevation and Width-Elevation Curves

First, a polygon was digitized surrounding each 2 km reach over 10 stations, as illustrated in Fig. 4, and a histogram was generated using SRTM elevations. The pixels (elevations) with considerably higher frequencies (for example, the frequency of pixels with water was about 2,000, whereas the frequency of pixels with the land was less than 200 in the case of Virtual station 1) were classified as the water areas and multiplied by 30×30 m (area of one SRTM pixel) for calculating the associated areas. In the case of the width, considering one pixel of the SRTM (30 m) along each river reach (Fig. 4), we digitized the polygon across the river and selected the water pixels following the same method as the area calculation. Next, the area-elevation/width-elevation curves were generated over those pixels in GEE. We opted for regression equations for each curve and found the best-fit regression equations to define the relationships between the area-elevation and width-elevation (Figs. 5 and 6).

Landsat-8 Based Water Area/Width Extraction

For assessing the elevations not captured by SRTM (Fig. 3), the best-fit regression equations were used for extrapolating area-elevation and width-elevation curves. The water area and width each averaged over a 2-km reach out of the 10 virtual river stations that were derived using the Modified Normalized Difference Water Index (MNDWI; Han-Qiu 2005). The MNDWI is defined as follows

$$\mathrm{MNDWI} = (\mathrm{green} - \mathrm{SWIR1})/(\mathrm{green} + \mathrm{SWIR1})$$

where green = green band; and SWIR1 = shortwave infrared band 1 for the Landsat 8 surface reflectance product. The pixels of MNDWI images with values less than zero were masked to derive the pixels associated with the water areas. The satellite radar altimeter ground track is a few kilometers wide. The elevation of the river surface estimated from the SRTM-Landsat technique was therefore averaged over a 2 km reach for this reason to derive a single value representative of the 2 km reach. This was then compared with the altimeter-based river elevations.

After an evaluation of the areas and reach-averaged width of all 10 stations, the corresponding elevations were calculated using the regression equations shown in Figs. 5 and 6, followed by

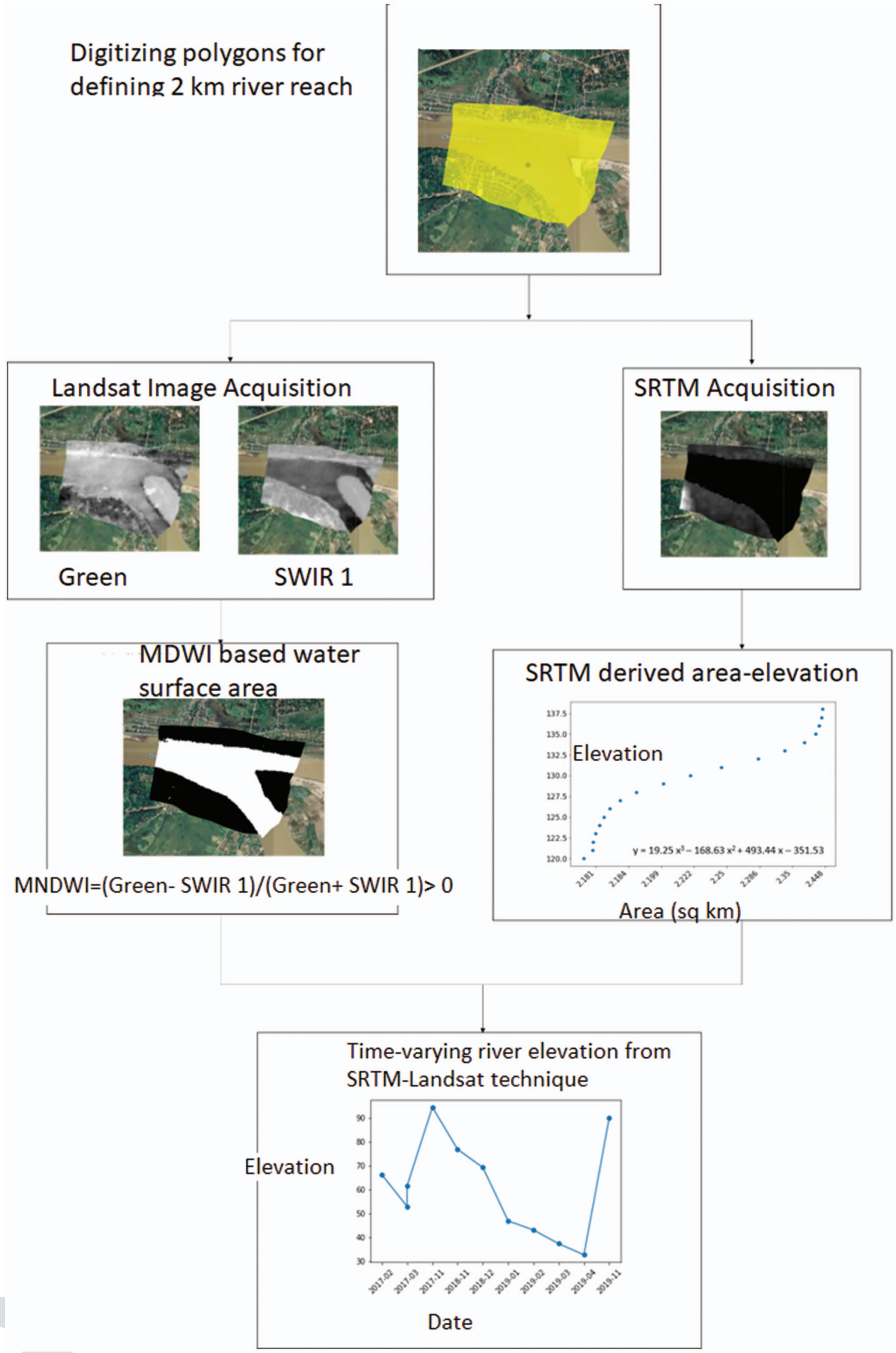

Fig. 2. (Color) Schematic showing combination of Landsat derived river area and SRTM derived area-elevation curve to generate time-varying river water elevations. The same methodology has been followed for the estimation of water elevations combining Landsat-derived river width and the SRTM derived width–elevation curve. (Landsat-8 base image courtesy of the US Geological Survey.)

extrapolating the area-elevation and width-elevation curves. Finally, these SRTM-Landsat based area-elevation and width-elevation relationships were used to derive the time-varying river elevations at Landsat overpass times from 2016 to 2019.

Water Heights Derived from Sentinel 3A and Jason 3 Altimeters

The time-varying elevations calculated using the SRTM-Landsat combined technique were verified using Sentinel 3A and Jason 3 altimeter data over the designated stations shown in Fig. 1. Jason 3 water surface elevation data were retrieved from the dynamic river width–based Altimeter Height Visualizer website of the SASWE research group (UW) from the web portal referenced by Biswas et al. (2019) and noted in the Data Availability statement. In this visualizer, Biswas et al. (2019) applied river extent information (river width and course) from visible (Landsat) and the synthetic aperture radar (SAR) platform (Sentinel-1) to extract elevations of water in South and South East Asia. The extent-based approach was applied to filter out nonwater radar returns using two methods: (1) the river mask (RM)–based K-means (KM) clustering (hence, RM + KM); and (2) K-means clustering embedded with the RM

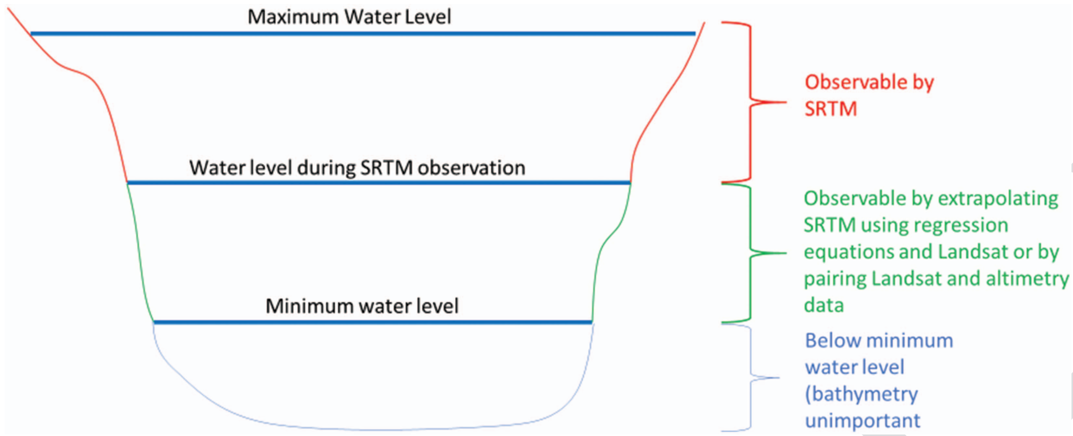

Fig. 3. (Color) Schematic showing water levels observable by SRTM and the unobserved river bathymetry.

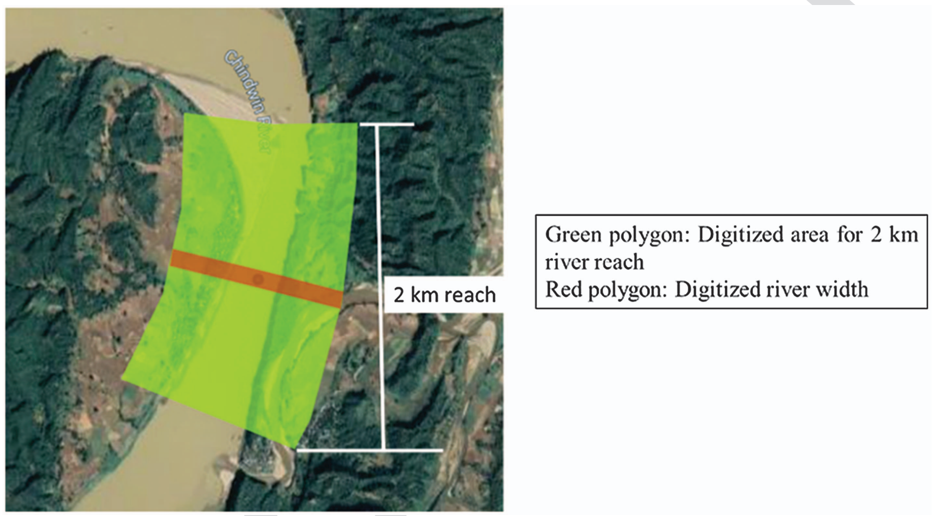

Fig. 4. (Color) Digitizing river area and width for SRTM area–elevation and width–elevation curve generation. (Landsat-8 base image courtesy of the US Geological Survey.)

(hence, KMRM). The incorporation of the river extent information was observed to be beneficial for highly varying seasonal widths.

After river elevation extraction, data closest to the overpass dates of the Landsat 8 imagery acquisition were considered. The independent set of time-varying water elevations from altimeters at the 10 virtual stations was plotted. The change of water elevation on each date from the previous date (as anomalies) was evaluated to observe the changing pattern for both our proposed SRTM-Landsat based water elevation time series and the independent altimeter-derived time series. Finally, the coefficients of correlation were evaluated between two sets of water elevation anomalies to verify the accuracy of our proposed SRTM-Landsat combined technique for time-varying water elevation extraction.

Results and Discussions

Regression Equations from SRTM-Based Area-Elevation and Width-Elevation Curves

Regression models were used to establish the relationship between the area/width and elevation obtained from the SRTM. The best-fit regression equations, along with the area-elevation and width-elevation curves, are represented in Figs. 5 and 6, respectively. In Figs. 5 and 6, the blue dots represent the values extracted from the SRTM. The orange dots represent the values derived using Landsat and the regression equations of the SRTM-based curves for deriving the lower portion of the bathymetry not observed by the SRTM during its overpass in February 2000. The variabilities of the SRTM-Landsat combined area-elevation and width-elevation curves for different reaches are almost similar; the values of water elevation increase with increasing areas and widths depending on the characteristics of bathymetry. The lower portions of the bathymetry for both area-elevation and width-elevation curves, derived using Landsat 8 images and regression relationships, are mostly linear in nature for the Chindwin River.

Comparison of SRTM-Landsat-Based Water Surface Elevations with Altimeter River Heights

The areas and widths extracted using the MNDWI (described in the section "Landsat-8 Based Water Area/Width Extraction") technique were first used to extrapolate the portion of area-elevation and width-elevation curves not observed by SRTM (Fig. 3). Next, the time

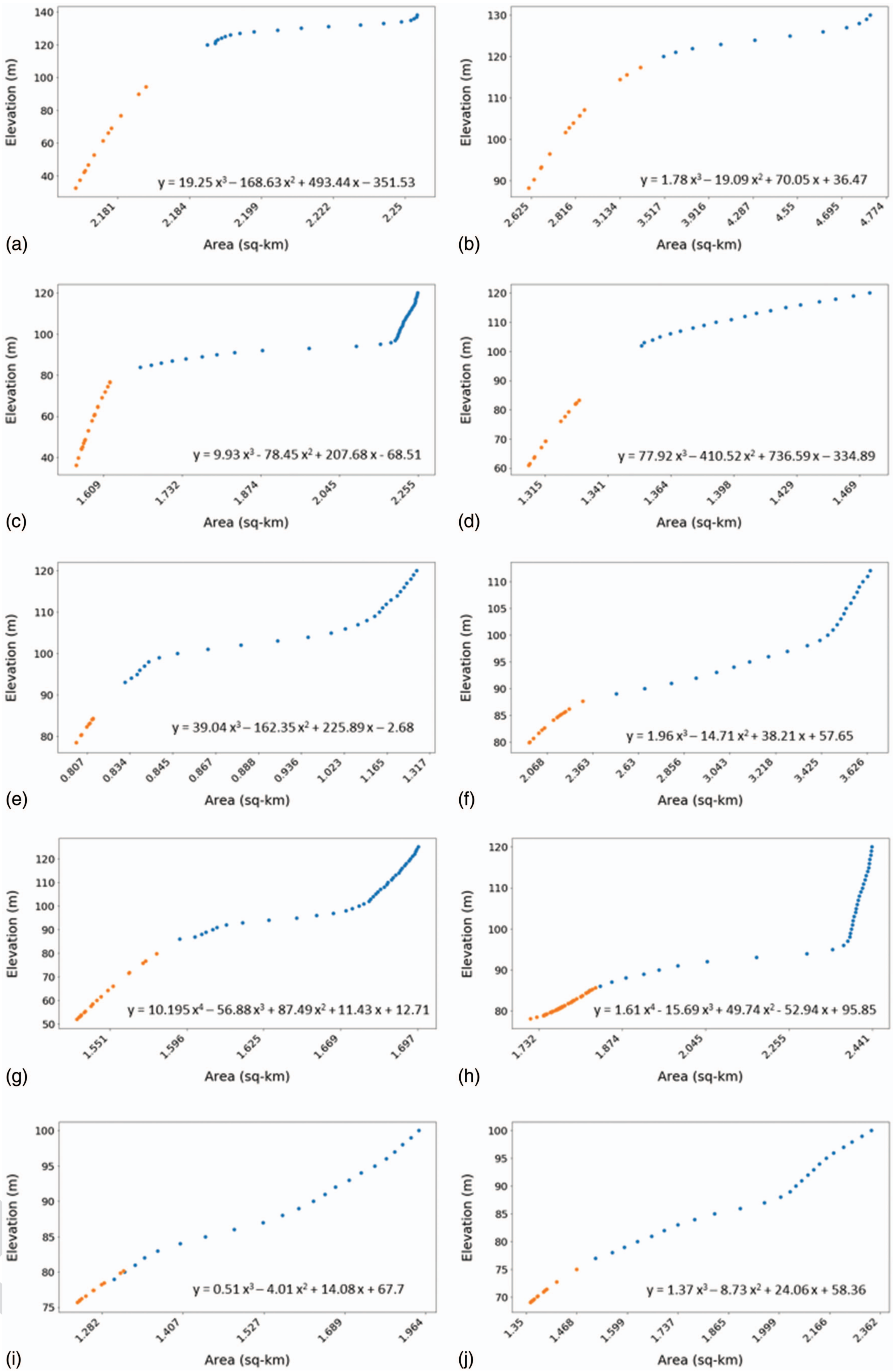

Fig. 5. (Color) SRTM-Landsat derived combined area–elevation curves and regression equations. In this study, the plots (a–j) are for virtual stations numbered from 1 to 10 of the Chindwin River, as shown in Fig. 1. The blue dots represent the values extracted from SRTM only, and the orange dots represent the values derived using Landsat and the regression equations of the SRTM-based curves. Regression equations are also given at the bottom of each plot.

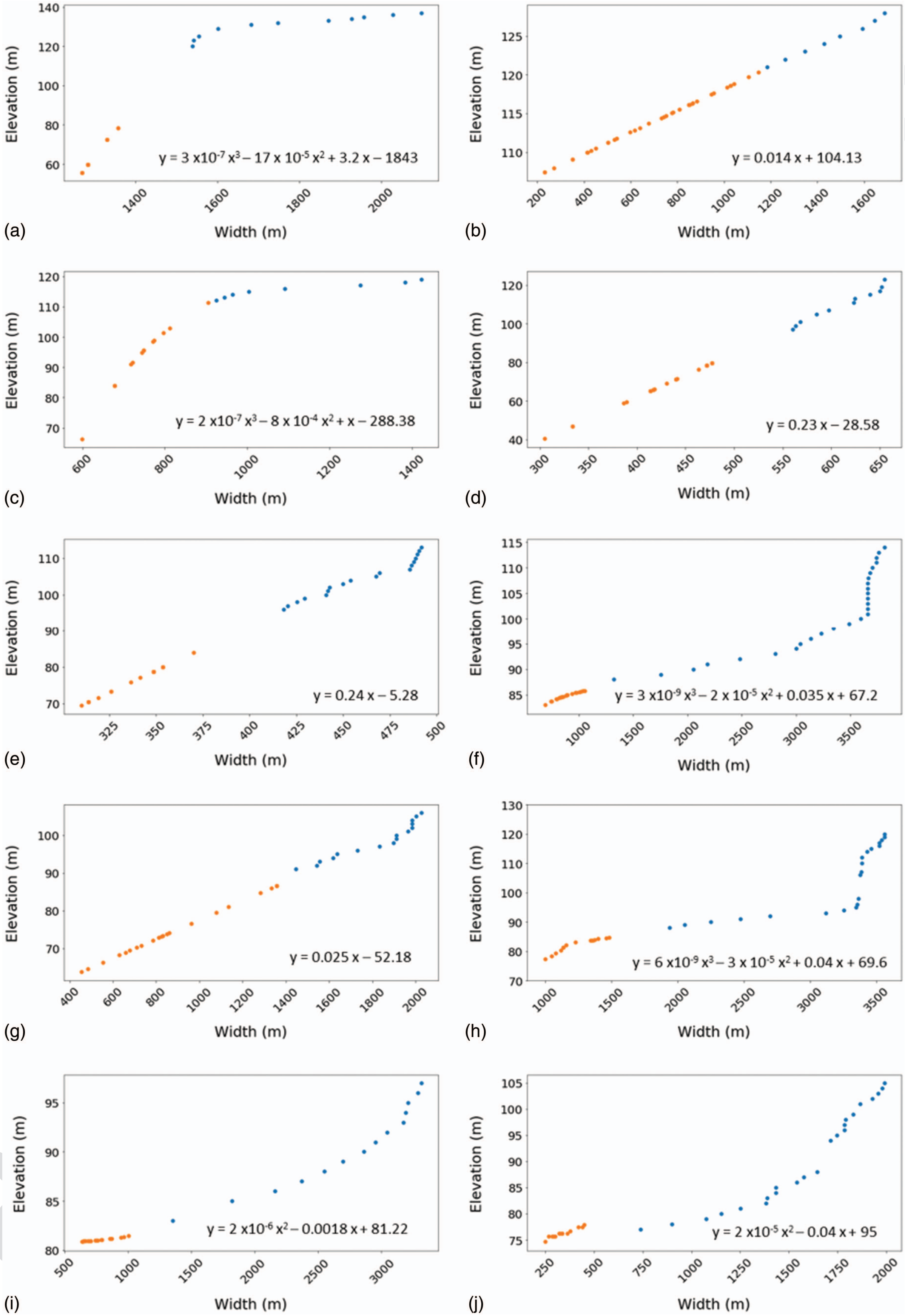

Fig. 6. (Color) SRTM-Landsat derived width–elevation curves and regression equations. In this study, the plots (a–j) represent virtual stations numbered from 1 to 10 of the Chindwin River, as shown in Fig. 1. The blue dots represent the values extracted from SRTM only, and the orange dots represent the values derived using Landsat and the regression equations of the SRTM-based curves. Regression equations are also given at the bottom of each plot.

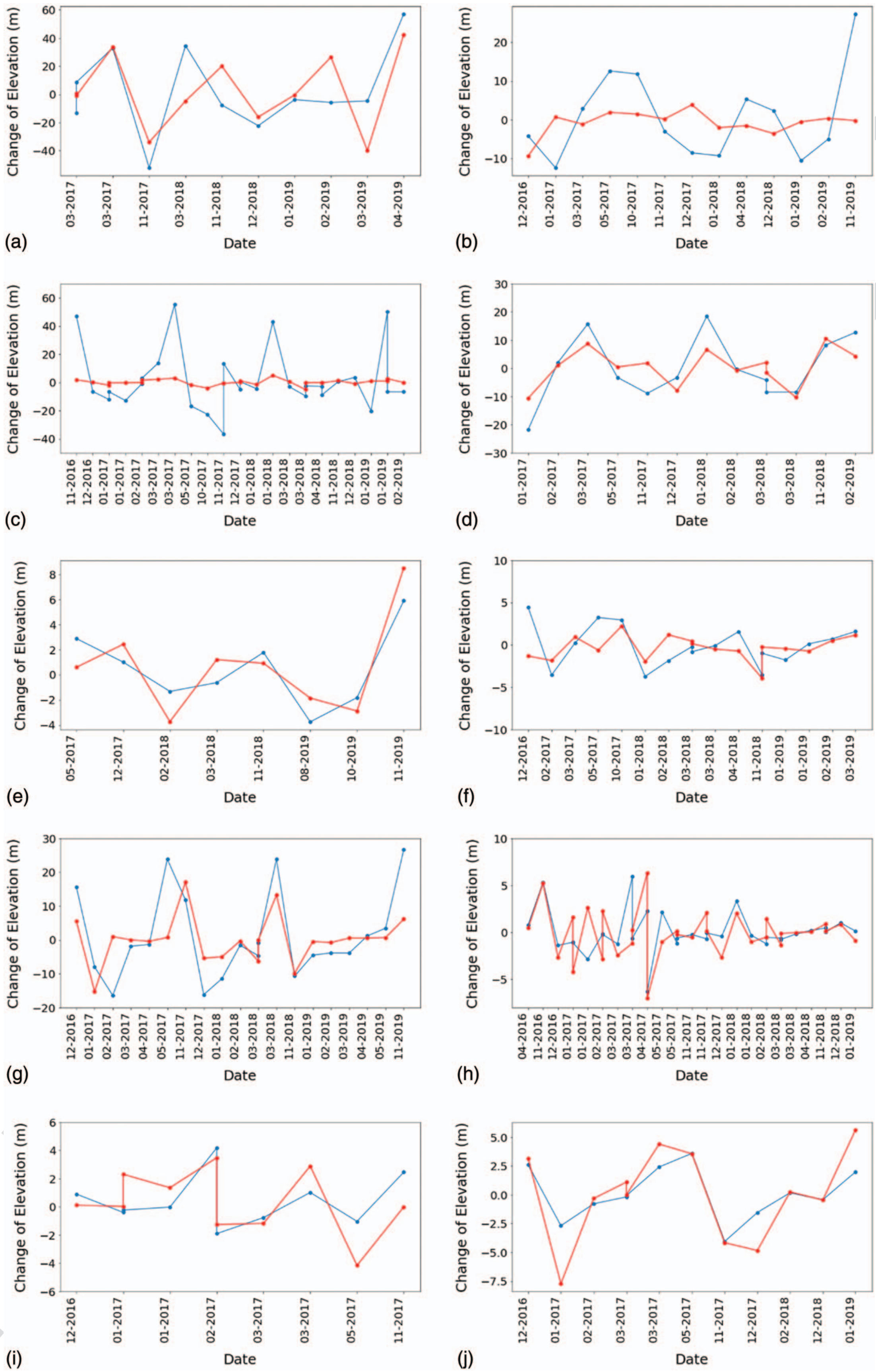

Fig. 7. (Color) Time series of change in water elevations from 2016 to 2019 for 2 km reach centering each virtual station as designated in Fig. 1. In this study, plots (a–j) correspond to stations 1 to 10, respectively, as shown in Fig. 1. The blue curves represent the change in elevations derived from SRTM-Landsat based area–elevation relationships, and the red curves represent the change in elevations from Sentinel 3A and JASON 3. The correlation coefficients are also given in each plot.

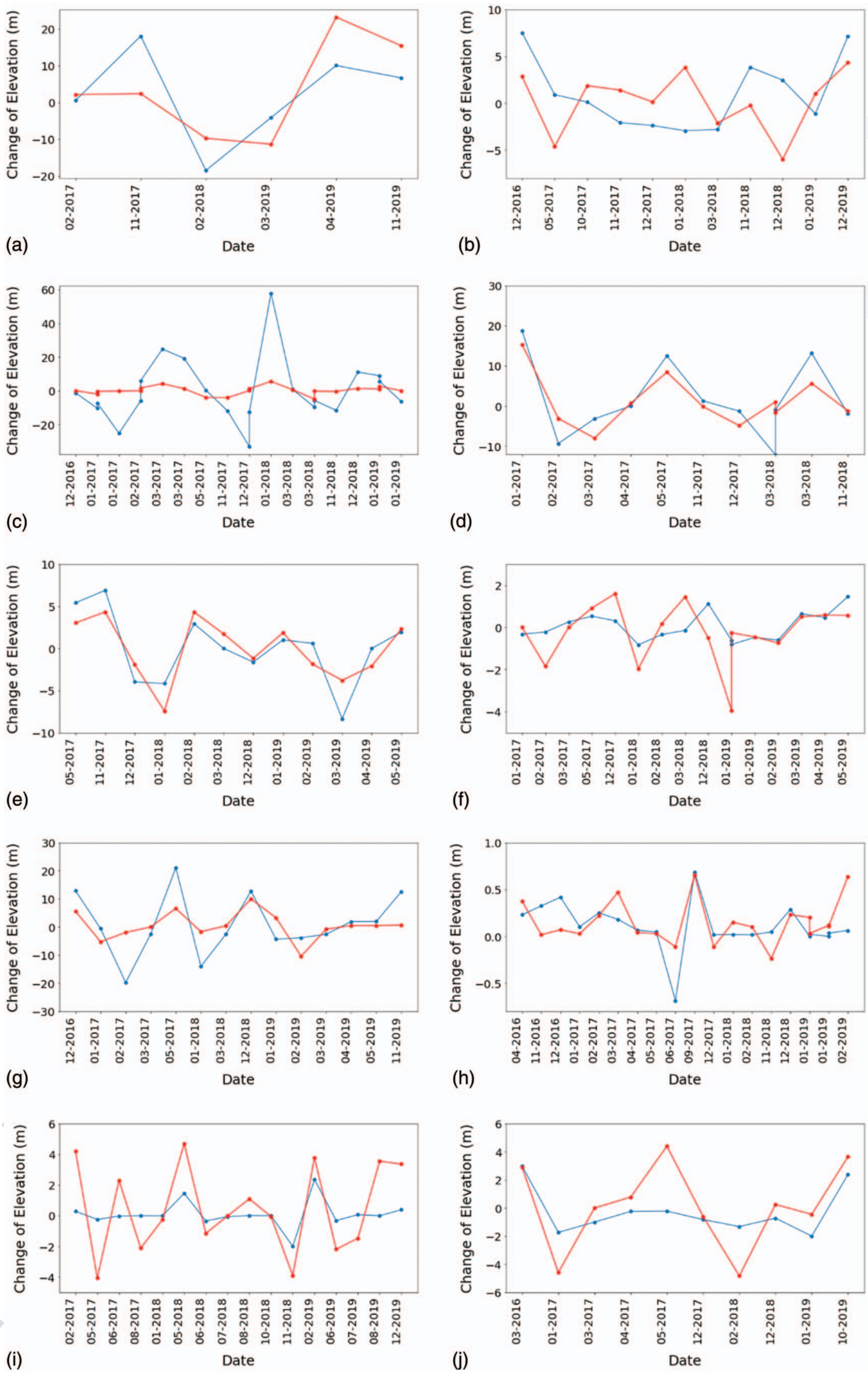

Fig. 8. (Color) Time series of change in water elevations from 2016 to 2019 for each virtual station as designated in Fig. 1. In this study, plots (a–j) correspond to virtual stations 1 to 10, respectively, as shown in Fig. 1. The blue curves represent the change in elevations derived from SRTM-Landsat based width–elevation relationships, and the red curves represent the change in elevations from Sentinel 3A and Jason 3. The correlation coefficients are also given in each plot.

series of elevations were generated using the SRTM-Landsat based area-elevation and width-elevation relationships, followed by verification using Sentinel 3A and Jason 3 derived water heights. As mentioned in the section "Water Heights Derived from Sentinel 3A and Jason 3 Altimeters," our proposed method was assessed by comparing the time series of water surface anomalies from 2016 to 2019, which are represented in Figs. 7 and 8. In those figures, the blue curves represent the change in elevations derived from SRTM-Landsat based relationships, whereas the red curves represent the change in elevations independently derived from Sentinel 3A and JASON 3.

Our results suggest that there is a strong correlation at most of the virtual stations between the water elevation changes derived using our proposed method and the changes derived independently from the altimeter river heights. The correlation coefficients between the water elevation change derived using the SRTM-Landsat area-elevation relationships and the change derived from altimeter heights vary from 0.10 to 0.89. Similarly, the correlation coefficients between the water elevation change derived using SRTM-Landsat width-elevation relationships and the change derived from altimeter heights vary from 0.20 to 0.82. Obviously, there is a wide range in how much of the variability the SRTM-Landsat technique can capture for river elevation changes, ranging from 20% to 80%. This wide range is not unexpected if one reviews recent literature. Studies reported by Legleiter and Harrison (2019) and Kasvi et al. (2019) are unanimous in challenges faced in estimating bathymetry for deeper rivers using the direct approach of penetration or at shallow rivers using water classification techniques (such as in this study). In fact, Kasvi et al. (2019) noted that more research is needed for shallow water bathymetry, which is consistent with our findings in this study when low correlations are reported for our SRTM-Landsat technique. There is a difference between the values of the two sets of elevation changes as suggested by the time-series plots in Figs. 7 and 8. This difference is speculated to be the reason for uncertainties involved in each satellite product, as well as the geophysical sources of errors, such as the presence of islands or shallow water (discussed subsequently and shown in Fig. 10). Barring the cases when the SRTM-Landsat method is not effective, such as narrow rivers with islands or sand bars, we do notice that the method captured the changes in the water elevation pattern well with respect to the altimeter heights. As shown in Fig. 7(j), the coefficient of correlation is 0.89, which means SRTM-Landsat combined elevation changes (extracted from the area-elevation relationship) can capture more than 80% of the elevation variability exhibited by the Sentinel 3A–derived water heights. For instance, from November 2016 to January 2017, the SRTM-Landsat based water surface elevation decreased very similarly to what was extracted from Sentinel 3A. Although there is a difference between the value of the water elevation, the SRTM-Landsat area-elevation approach is able to capture the same decrease in the water surface elevation. Similarly, if we notice Fig. 8(e), the coefficient of correlation is 0.82, which means the SRTM-Landsat combined elevation changes are strongly correlated to the Sentinel 3A–derived water heights. For instance, from May 2017 to November 2017, the water surface elevation increased according to the Sentinel 3A water heights. The SRTM-Landsat width-elevation relationship also captured that increase in the water surface elevation.

In general, the correlations between the change of water elevations derived from altimeters and our proposed SRTM-Landsat approach are found to be stronger in the case of river reaches with relatively smaller areas and widths where there is unlikely to be river islands. The correlation between the water surface anomalies derived using the SRTM-Landsat area-elevation relationships and altimeter heights are weak (0.1 and 0.46, respectively) in the case of Stations 2 and 6 [Figs. 7(b and f)] compared to the other eight stations. The maximum water area from 2016 to 2019 for these two stations is approximately 2.2 km^2, which is greater than the areas of the other eight stations. Similarly, the correlation between water surface anomalies derived using SRTM-Landsat width-elevation relationships and altimeter heights are weak (0.20 and 0.49, respectively) in the case of Stations 2 and 6 [Figs. 8(b and f)] compared to the other eight stations. The maximum width from 2016 to 2019 for these two stations is approximately 1,100 m, which is greater than the widths of Stations 4, 5, 9, and 10 but smaller than Stations 1, 3, 7, and 8. These relationships are represented in Fig. 9, which clearly defines that with the increasing area of each station, the correlation between the two datasets decreases. There are three clear thresholds observed in Fig. 9(a). When the water area is less than 1.2 km^2, the correlation is very strong, with values 0.80 to 0.89. Between water area areas of ∼1.2 to ∼1.8 km^2, there exists a moderate correlation ranging from 0.52 to 0.67, while stations with areas greater than ∼1.8 km^2 show weak correlations.

Fig. 9(b) represents that for the stations with widths less than 500 m, the correlations between the water elevation changes from SRTM-Landsat, and the altimeters are strong, with values ranging from 0.71 to 0.82 (Stations 4, 5, and 10). The stations with widths greater than 500 m show moderate correlation, among which Stations 6 and 2 are with a minimum correlation, as mentioned

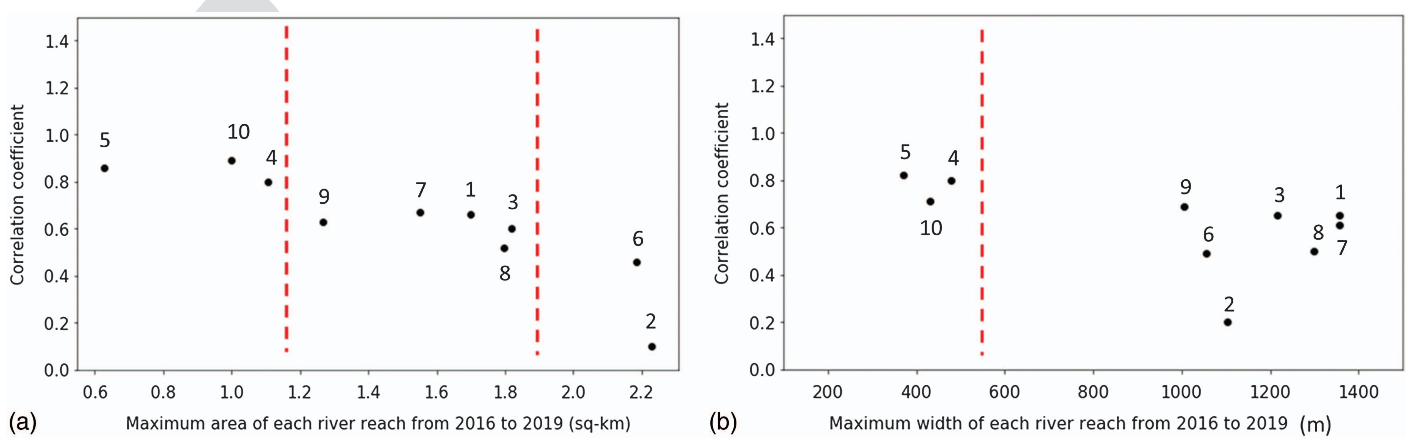

F9:1 **Fig. 9.** (Color) Relationships between (a) correlation coefficient and maximum area; and (b) correlation coefficient and maximum width for each
F9:2 station during 2016 to 2019. The numbers above each dot refer to the station number mentioned in Fig. 1.

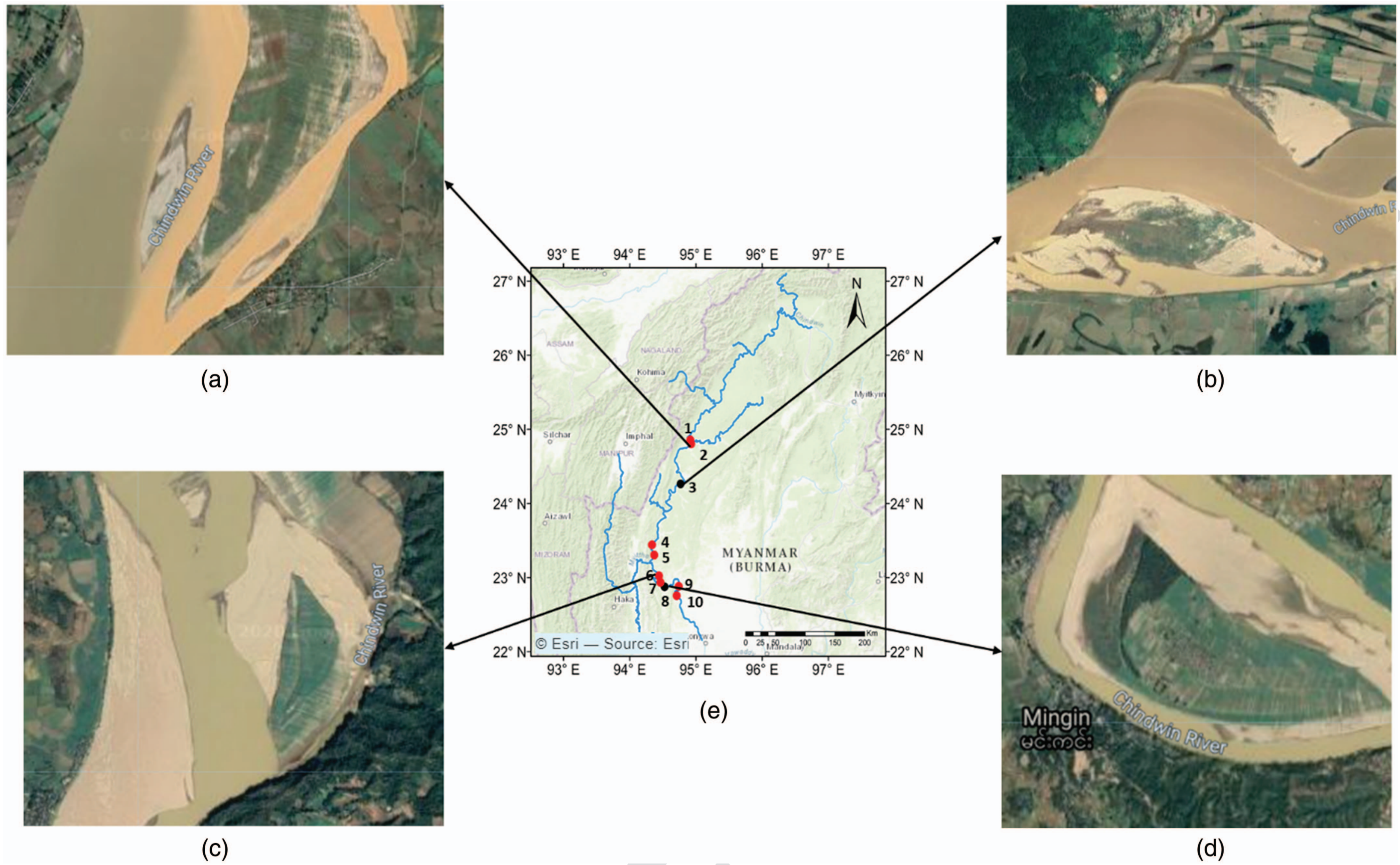

Fig. 10. (Color) Landsat-8 imagery of 2 km reaches showing dry season river deltas within (a) Station 2; (b) Station 3; (c) Station 6; and (d) Station 8, as mentioned in Fig. 1. [(a–d) Landsat-8 images courtesy of the US Geological Survey; (e) Map © Esri.]

previously. After forensically analyzing the Landsat-8 imagery, the stations with a larger width where the river is braided with river deltas yield poor correlations (Fig. 10). This finding is consistent with recent studies reported by Kasvi et al. (2019), in which shallow water bathymetry in wide rivers appears to be challenging for remote sensing techniques. These river deltas get exposed during the dry season but are submerged in the monsoon season. Hence, we can speculate that it is not only the larger water areas and widths but also the presence of deltas during the dry season that undermines our proposed SRTM-Landsat combined technique. For instance, if we consider Station 2 as shown in Fig. 9(b), the width of this section (~1,100 m) is smaller than Station 7 (~1,300 m), but as there is a river delta in Station 2 (Fig. 10), the correlation value is lower than Station 7.

Conclusions

This study explored the capability of an SRTM-Landsat remote sensing technique for estimating time-varying water elevation for the Chindwin River in Myanmar. In this study, the area-elevation and width-elevation curves were derived from SRTM and developed the best-fit regression equations using a regression model over 10 virtual stations of the Chindwin River in Myanmar. These stations were also sampled by Sentinel 3A and Jason 3 satellite radar altimeter tracks. A comparison of our proposed SRTM-Landsat based elevation change with Sentinel 3A/Jason 3-based elevation changes resulted in a correlation coefficient up to 0.89. The river reaches with smaller areas and widths are likely to be more reliable for our proposed SRTM-Landsat method. Stations with weaker correlations often corresponded to the braided portion of the river reach, where the river deltas get exposed during the dry season and are inundated during the monsoon season. As a first-cut that is simple and globally applicable due to the use of widely available datasets (SRTM and Landsat), our proposed technique over the Chindwin River showed acceptable promise in characterizing river bathymetry and time-varying river heights.

Our study is not without limitations. One area of further study is the role of spatial resolution of topography from satellite remote sensing to understand the impact on estimating river bathymetry. In this study, the highest resolution DEM that is globally and freely available has been used from the SRTM mission at 30 m. For rivers in Southeast Asia, such as the Chindwin River, land elevation and riverine regions tend to have flat topography, making SRTM DEM sometimes ineffective. For example, SRTM DEM is known to have nonnegligible uncertainty that has been consequently addressed in recent DEM products by Yamazaki et al. (2017). A higher resolution DEM, such as one from a LIDAR survey, can be expected to yield a more accurate estimate of river elevations. However, LIDAR data on topography is not globally or publicly available. The goal of this study was to develop a technique that could serve as a first-cut based on publicly available datasets global in scope. During the initial stages of any hydrodynamic model effort at ungauged river basins, our proposed SRTM-Landsat technique can bridge the first gap between data requirements in hydrologic/hydrodynamic simulations and in situ data availability for river heights. Consequently, with a further survey or use of additional data and complex methods, such work can enhance flood risk management efforts, such as for the Chindwin basin that is prone to flooding. We do not propose our method as the final word on river bathymetry and river height estimation at ungauged locations but rather as the initial baseline that can be rapidly derived cost-effectively when an expensive and quality-controlled survey or remote sensing data are unavailable promptly to the river modeling community.

Data Availability Statement

All data, models, and code generated or used during the study appear in the published article. The Dynamic River Width based Altimeter Height Visualizer website of the SASWE research group (UW) can be accessed at http://depts.washington.edu/saswe/jason3. Landsat-8 data was courtesy of the USGS (https://www.usgs.gov/core-science-systems/nli/landsat). STRM and Jason-3 data was courtesy of NASA/JPL-Caltech (https://www2.jpl.nasa.gov/srtm/ and https://www.jpl.nasa.gov/missions/jason-3, respectively). Sentinel-3A data was courtesy of NOAA (https://coastwatch.noaa.gov/cw/satellite-data-products/ocean-color/near-real-time/olci-sentinel3-global.html).

Acknowledgments

The authors gratefully acknowledge support from the National Aeronautics and Space Administration (NASA) Applied Sciences NNX16AQ54G that allowed the University of Washington to engage and train at the Asian Disaster Preparedness Center (ADPC) as a Surface Water Ocean Topography (SWOT) Satellite Mission Early Adopter. The work was supported by the generous contributions from the University of Washington Global Affairs and The Ivanhoe Foundation.

References

Andreadis, K. M., G. J.-P. Schumann, and T. Pavelsky. 2013. "A simple global river bankfull width and depth database." *Water Resour. Res.* 49 (10): 7164–7168. https://doi.org/10.1002/wrcr.20440.

Arsen, A., J.-F. Crétaux, and R. Abarca del Rio. 2015. "Use of SARAL/AltiKa over mountainous lakes, intercomparison with Envisat mission." Supplement, *Mar. Geod.* 38 (S1): 534–548. https://doi.org/10.1080/01490419.2014.1002590.

Aviso. 2020. "Radar altimetry tutorial and toolbox." Accessed September 29, 2020. http://www.altimetry.info/radar-altimetry-tutorial/how-altimetry-works/basic-principle/.

Bates, P. D., J. C. Neal, D. Alsdorf, and G. J.-P. Schumann. 2013. "Observing global surface water flood dynamics." In *The earth's hydrological cycle*, 839–852. Dordrecht, Netherlands: Springer.

Bercher, N., and P. Kosuth. 2012. "Monitoring river water levels from space: Quality assessment of 20 years of satellite altimetry data." In [10] *Proc., 20 Years of Progress in Radar Altimetry*, 24–29.

Biancamaria, S., D. P. Lettenmaier, and T. M. Pavelsky. 2016. "The SWOT mission and its capabilities for land hydrology." *Surv. Geophys.* 37 (2): 307–337. https://doi.org/10.1007/s10712-015-9346-y.

Biancamaria, S., T. Schaedele, D. Blumstein, F. Frappart, F. Boy, J.-D. Desjonquères, C. Pottier, F. Blarel, and F. Niño. 2018. "Validation of Jason-3 tracking modes over French rivers." *Remote Sens. Environ.* 209 (May): 77–89. https://doi.org/10.1016/j.rse.2018.02.037.

Birkinshaw, S. J., G. M. O'Donnell, P. Moore, C. G. Kilsby, H. J. Fowler, and P. A. M. Berry. 2010. "Using satellite altimetry data to augment flow estimation techniques on the Mekong River." *Hydrol. Processes* 24 (26): 3811–3825. https://doi.org/10.1002/hyp.7811.

Biswas, N. K., F. Hossain, M. Bonnema, M. A. Okeowo, and H. Lee. 2019. "An altimeter height extraction technique for dynamically changing rivers of South and South-East Asia." *Remote Sens. Environ.* 221 (Feb): 24–37. https://doi.org/10.1016/j.rse.2018.10.033.

Boergens, E., S. Buhl, D. Dettmering, C. Klüppelberg, and F. Seitz. 2017. "Combination of multi-mission altimetry data along the Mekong River with spatio-temporal kriging." *J. Geod.* 91 (5): 519–534. https://doi.org/10.1007/s00190-016-0980-z.

Gao, H., S. Zhang, M. Durand, and H. Lee. 2016. "Satellite remote sensing of lakes and wetlands." In *Hydrologic remote*, 57–72. Boca Raton, FL: CRC Press.

GEE. 2020. "Earth engine data catalog, Google developers." Accessed July 31, 2020. https://developers.google.com/earth-engine/datasets/catalog. [11] [12]

Getirana, A. C. V., and C. Peters-Lidard. 2013. "Estimating water discharge from large radar altimetry datasets." *Hydrol. Earth Syst. Sci.* 17 (3): 923–933. https://doi.org/10.5194/hess-17-923-2013.

Han-Qiu, X. U. 2005. "A study on information extraction of water body with the modified normalized difference water index (MNDWI)." *J. Remote Sens.* 5: 589–595. [13] [14]

Huang, C., B. D. Nguyen, S. Zhang, S. Cao, and W. Wagner. 2017. "A comparison of terrain indices toward their ability in assisting surface water mapping from Sentinel-1 data." *ISPRS Int. J. Geo-Inf.* 6 (5): 140. https://doi.org/10.3390/ijgi6050140.

Jiang, L., K. Nielsen, S. Dinardo, O. B. Andersen, and P. Bauer-Gottwein. 2020. "Evaluation of Sentinel-3 SRAL SAR altimetry over Chinese rivers." *Remote Sens. Environ.* 237 (Feb): 111546. https://doi.org/10.1016/j.rse.2019.111546.

Karpatne, A., A. Khandelwal, X. Chen, V. Mithal, J. Faghmous, and V. Kumar. 2016. "Global monitoring of inland water dynamics: State-of-the-art, challenges, and opportunities." In *Computational sustainability*, 121–147. Cham, Switzerland: Springer.

Kasvi, E., J. Salmela, E. Lotsari, T. Kumpula, and S. N. Lane. 2019. "Comparison of remote sensing based approaches for mapping bathymetry of shallow, clear water rivers." *Geomorphology* 333 (May): 180–197. https://doi.org/10.1016/j.geomorph.2019.02.017.

Kittel, C. M., L. Jiang, C. Tøttrup, and P. Bauer-Gottwein. 2021. "Sentinel-3 radar altimetry for river monitoring—A catchment-scale evaluation of satellite water surface elevation from Sentinel-3A and Sentinel-3B." *Hydrol. Earth Syst. Sci.* 25 (1): 333–357. https://doi.org/10.5194/hess-25-333-2021.

Kittel, C. M., K. Nielsen, C. Tøttrup, and P. Bauer-Gottwein. 2018. "Informing a hydrological model of the Ogooué with multi-mission remote sensing data." *Hydrol. Earth Syst. Sci.* 22 (2): 1453. https://doi.org/10.5194/hess-22-1453-2018.

Kleinherenbrink, M., R. C. Lindenbergh, and P. G. Ditmar. 2015. "Monitoring of lake level changes on the Tibetan Plateau and Tian Shan by retracking Cryosat SARIn waveforms." *J. Hydrol.* 521 (Feb): 119–131. https://doi.org/10.1016/j.jhydrol.2014.11.063. [15]

Kumar, M., S. Chidambaram, A. L. Ramanathan, R. Goswami, and S. Eslamian. 2015. "Criterion, indices, and classification of water quality and water reuse options." In Chap. 13 of *Urban water reuse handbook*, edited by S. Eslamian, 163–176. Boca Raton, FL: Taylor and Francis, CRC Group.

Legleiter, C. J., and L. R. Harrison. 2019. "Remote sensing of river bathymetry: Evaluating a range of sensors, platforms, and algorithms on the upper Sacramento River, California, USA." *Water Resour. Res.* 55 (3): 2142–2169. https://doi.org/10.1029/2018WR023586.

Liu, G., F. W. Schwartz, K.-H. Tseng, and C. K. Shum. 2015. "Discharge and water-depth estimates for ungauged rivers: Combining hydrologic, hydraulic, and inverse modeling with stage and water-area measurements from satellites." *Water Resour. Res.* 51 (8): 6017–6035. https://doi.org/10.1002/2015WR016971.

Maswood, M., and F. Hossain. 2016. "Advancing river modelling in ungauged basins using satellite remote sensing: The case of the Ganges–Brahmaputra–Meghna basin." *Int. J. River Basin Manage.* 14 (1): 103–117. https://doi.org/10.1080/15715124.2015.1089250.

Moramarco, T., S. Barbetta, D. Bjerklie, J. W. Fulton, and A. Tarpanelli. 2019. "River bathymetry estimate and discharge assessment from remote sensing." *Water Resour. Res.* 55 (8): 6692–6711. https://doi.org/10.1029/2018WR024220.

Neal, J., G. J. P. Schumann, and P. D. Bates. 2018. "A simple model for simulating river hydraulics and floodplain inundation over large and data sparse areas." *Water Resour. Res.* 48. [16] [17]

Paiva, R. C., M. T. Durand, and F. Hossain. 2015. "Spatiotemporal interpolation of discharge across a river network by using synthetic SWOT satellite data." *Water Resour. Res.* 51 (1): 430–449. https://doi.org/10.1002/2014WR015618.

Pavlis, N. K., S. A. Holmes, S. C. Kenyon, and J. K. Factor. 2012. "The development and evaluation of the Earth Gravitational Model 2008 (EGM2008)." *J. Geophys. Res. Solid Earth* 117 (4). https://doi.org/10.1029/2011JB008916.

Sauer, V. B., and D. P. Turnipseed. 2010. *Stage measurement at gaging stations*. Washington, DC: US Dept. of the Interior, USGS.

Schumann, G., P. Matgen, M. E. J. Cutler, A. Black, L. Hoffmann, and L. Pfister. 2008. "Comparison of remotely sensed water stages from LiDAR, topographic contours and SRTM." *ISPRS J. Photogramm. Remote Sens.* 63 (3): 283–296. https://doi.org/10.1016/j.isprsjprs.2007.09.004.

Schumann, G. J. P., K. M. Andreadis, and P. D. Bates. 2014. "Downscaling coarse grid hydrodynamic model simulations over large domains." *J. Hydrol.* 508 (Jan): 289–298. https://doi.org/10.1016/j.jhydrol.2013.08.051.

Schumann, G. J.-P., P. D. Bates, G. Di Baldassarre, and D. C. Mason. 2012. "The use of radar imagery in riverine flood inundation studies." *Fluv. Remote Sens. Sci. Manage.* 115–140.

Shrestha, S., S. K. Gunawardana, T. Piman, and M. S. Babel. 2020. "Assessment of the impact of climate change and mining activities on streamflow and selected metal's loading in the Chindwin River, Myanmar." *Environ. Res.* 181 (Feb): 108942. https://doi.org/10.1016/j.envres.2019.108942.

Villadsen, H., O. B. Andersen, L. Stenseng, K. Nielsen, and P. Knudsen. 2015. "CryoSat-2 altimetry for river level monitoring—Evaluation in the Ganges–Brahmaputra River basin." *Remote Sens. Environ.* 168 (Oct): 80–89. https://doi.org/10.1016/j.rse.2015.05.025.

Yamazaki, D., D. Ikeshima, R. Tawatari, T. Yamaguchi, F. O'Loughlin, J. C. Neal, C. C. Sampson, S. Kanae, and P. D. Bates. 2017. "A high accuracy map of global terrain elevations." *Geophys. Res. Lett.* 44: 5844–5853. https://doi.org/10.1002/2017GL072874.

Yan, K., G. D. Baldassarre, D. P. Solomatine, and G. J.-P. Schumann. 2015. "A review of low-cost space-borne data for flood modelling: Topography, flood extent and water level." *Hydrol. Processes* 29 (15): 3368–3387. https://doi.org/10.1002/hyp.10449.

Queries

1. Please provide the ASCE Membership Grades for the authors who are members.

2. Please provide author titles (e.g., Professor, Director) for all affiliation footnotes.

3. Please check the hierarchy of section heading levels.

4. ASCE Open Access: Authors may choose to publish their papers through ASCE Open Access, making the paper freely available to all readers via the ASCE Library website. ASCE Open Access papers will be published under the Creative Commons-Attribution Only (CC-BY) License. The fee for this service is USD 2,000 and must be paid prior to publication. If you indicate Yes, you will receive a follow-up message with payment instructions. If you indicate No, your paper will be published in the typical subscribed-access section of the Journal. After a journal article is published, its copyright status cannot change until two years have passed. For further information, please see https://ascelibrary.org/page/openaccessoptionsandrights.

5. The citation (Bonnema et al. 2016) mentioned in this sentence is not present in the References list. Please provide the full details and we will insert it in the References list and link it to this citation.

6. The citation (Bonnema and Hossain 2017) mentioned in this sentence is not present in the References list. Please provide the full details and we will insert it in the References list and link it to this citation.

7. Please check all figures, figure citations, and figure captions to ensure they match and are in the correct order.

8. Please provide the expanded term for SASWE.

9. Per ASCE style, all websites should be listed in the References list. Please provide full reference information for any website listed in the text. We will include it in the References list and link it to citations in the text.

10. Please provide the publisher or sponsor name and location (not the conference location) for Bercher and Kosuth (2012).

11. Please provide the expansion for the term "GEE" for reference GEE (2020).

12. This reference GEE (2020) is not mentioned anywhere in the text. ASCE style requires that entries in the References list must be cited at least once within the paper. Please indicate a place in the text, tables, or figures where we may insert a citation or indicate if the entry should be deleted from the References list.

13. This query was generated by an automatic reference checking system. This reference could not be located in the databases used by the system. While the reference may be correct, we ask that you check it so we can provide as many links to the referenced articles as possible.

14. Please provide the issue number for Han-Qiu (2005).

15. This reference Kleinherenbrink et al. (2015) is not mentioned anywhere in the text. ASCE style requires that entries in the References list must be cited at least once within the paper. Please indicate a place in the text, tables, or figures where we may insert a citation or indicate if the entry should be deleted from the References list.

16. Please provide the issue number and page range for Neal et al. (2018).

17. This query was generated by an automatic reference checking system. This reference could not be located in the databases used by the system. While the reference may be correct, we ask that you check it so we can provide as many links to the referenced articles as possible.

18. Please provide the page range for Pavlis et al. (2012).

19. This query was generated by an automatic reference checking system. This reference could not be located in the databases used by the system. While the reference may be correct, we ask that you check it so we can provide as many links to the referenced articles as possible.

20. Please provide the volume and issue number for Schumann et al. (2012).

21. This reference Villadsen et al. (2015) is not mentioned anywhere in the text. ASCE style requires that entries in the References list must be cited at least once within the paper. Please indicate a place in the text, tables, or figures where we may insert a citation or indicate if the entry should be deleted from the References list.

22. Please provide the issue number for Yamazaki et al. (2017).